Practical aspects of thermomechanical modeling in electronics packaging
A case study with a SiC power package

Ye, Guigen; Fan, Xuejun; Zhang, Guoqi

DOI
10.1016/j.microrel.2022.114514

Publication date
2022

Document Version
Final published version

Published in
Microelectronics Reliability

Microelectronics Reliability 132 (2022) 114514

Contents lists available at ScienceDirect

Microelectronics Reliability

journal homepage: www.elsevier.com/locate/microrel

Practical aspects of thermomechanical modeling in electronics packaging: A case study with a SiC power package

Guigen Ye [a,*], Xuejun Fan [b,*], Guoqi Zhang [c]

[a] Department of Engineering Mechanics, China University of Petroleum (East China), Qingdao, China
[b] Department of Mechanical Engineering, Lamar University, PO Box 10028, Beaumont, TX 77710, USA
[c] Electronic Components, Technology and Materials, Faculty of Electrical Engineering, Delft University of Technology, Mekelweg 4, 2628CD Delft, the Netherlands

ARTICLE INFO

Keywords:
Finite element analysis
Thermomechanical modeling
Homogenization
Stress singularity
Volume averaging
Power package

ABSTRACT

In this paper, we presented several practical aspects for building robust and reliable finite element models in thermomechanical modeling in electronics packaging using finite element analysis. Firstly, for layered or patterned structures, a homogenized equivalent model, with equivalent orthotropic material properties, gives excellent agreement with the exact finite element model solutions. Such a simplified finite element model provides an efficient way for structural parameter optimization. Secondly, the finite element mesh should keep the fixed size and shape at the location of interest where the singular point exists. This approach provides a simple way for relative stress comparison in different designs, although the absolute value of stress components has no actual meaning. Thirdly, to further eliminate the mesh dependency, the volume averaging method can be used. We extended the local volume averaging method for large-area die attach problems. Fourthly, in this paper, we presented a comparison study between linear elastic and nonlinear viscoplastic analysis, and demonstrated that in some cases, two different types of analysis give opposite trend results. Lastly, we demonstrated that with the use of different stress components, the conclusions may be different. We also provided an ANSYS APDL script in the supplemental material as a benchmark example.

1. Introduction

The ever-expanding digitalization, driven by 5G, IoT to IoE, smart devices, data to cloud, and autonomous vehicles, is fast changing the electronics industry landscape. Consequently, advanced packaging has emerged, such as 2D, 2.1D, 2.3D, 2.5D, and 3D IC integration, using through-silicon via (TSV) interposer, or TSV-less, fan-out, and other interconnect technology. Numerous integration methods and fabrication techniques have been developed [1–3]. Furthermore, heterogeneous integration (HI) brings a new revolution for microelectronics packaging in the post-Moore era. HI becomes essential to provide higher performance and improved functionality with lower cost. Heterogeneity and associated integration are far-reaching and can relate to materials, component type, circuit type, node, interconnect method, and source or origin. HI also provides significant advantages to power delivery devices, as it permits the integration of wide bandgap (WBG) power devices, e.g., SiC, with silicon control, logic, and memory devices, and with evolving passive devices [4].

HI through system-in-package (SiP) builds large and complex systems out of simpler packages. A typical microelectronics package contains a number of interfaces with dissimilar materials [5]. The bonded interfaces are subjected to thermal stresses caused by the variation of temperature during operation, due to the different coefficients of thermal expansion (CTE). The thermomechanical stresses cause the degradation of the weaker interfaces or components of the integrated system, leading to device failure [4–11]. With SiC chip(s), which can sustain higher junction temperature, much more severe thermal stress could be induced. Therefore, thermomechanical reliability of a SiC-based electronics package becomes more important.

Thermomechanical modeling based on finite element analysis (FEA) (or, finite element modeling (FEM)) is one of the most important approaches for reliability evaluation and design optimization. Thermomechanical modeling helps to locate the regions that are most prone to failure, and compare and quantify reliability offered by different integration designs. The role and influence of thermomechanical modeling have been extensively studied [4–10,12]. A linear elastic finite element analysis is generally a first step to approximately estimate the stress and deformation behavior. However, it must be noted that further nonlinear analysis may in some cases provide opposite trend results [5,6]. In

* Corresponding authors.
E-mail addresses: yegg@upc.edu.cn (G. Ye), xuejun.fan@lamar.edu (X. Fan).

https://doi.org/10.1016/j.microrel.2022.114514
Received 7 October 2021; Received in revised form 30 January 2022; Accepted 7 March 2022
Available online 18 March 2022

Nomenclature

English alphabet

E_z	Equivalent longitudinal Young's modulus
E_x, E_y	Equivalent transverse Young's modulus
G_{xz},G_{yz}	Equivalent longitudinal shear modulus
G_{xy}	Equivalent transverse shear modulus
a_x, a_y	Equivalent transverse CTEs
a_z	Equivalent longitudinal CTE
E_{Cu}	Elastic Young's modulus of Cu
E_{Ag}	Elastic Young's modulus of sintered Ag
G_{Cu}	Shear modulus of Cu
G_{Ag}	Shear modulus of sintered Ag
a_{Cu}	CTE of Cu
a_{Ag}	CTE of sintered Ag
V_{Cu}	Volume fraction of Cu

Greek alphabet

ν_{xz},ν_{yz}	Equivalent longitudinal Poisson ratio
ν_{xy}	Equivalent transverse Poisson ratio
ν_{Cu}	Poisson ratio of Cu
ν_{Ag}	Poisson ratio of Ag
ξ_E	Geometry parameter for Young's modulus
ξ_G	Geometry parameter for shear modulus
ξ_ν	Geometry parameter for Poisson ratio

Parameter combination

η_E	$(E_{Cu}/E_{Ag} - 1)/(E_{Cu}/E_{Ag} + \xi_E)$
η_G	$(G_{Cu}/G_{Ag} - 1)/(G_{Cu}/G_{Ag} + \xi_G)$
η_ν	$(\nu_{Cu}/\nu_{Ag} - 1)/(\nu_{Cu}/\nu_{Ag} + \xi_\nu)$

addition to the type of analysis and material model to be used, the choice of a robust finite element mesh is critical for thermomechanical modeling [7]. The meshing quality significantly affects the accuracy of simulation results. It is generally believed that when the mesh size decreases to a certain extent the simulation tends to be converged and the results become mesh-independent [13]. However, there exist free edges of the bonded dissimilar materials or angular corners of a wedge-shape in a packaging assembly. Stress singularity occurs at these free-edges and wedge corners [9]. Suhir [14] and Tsai et al. [15] theoretically proved the existence of the singularity for both the shear and normal stress at the free edge in elastic analysis. And the singular stress field at the free ends of interfaces were predicted even when with an inelastic analysis [16,17]. The stress singularity means the stress values at the singular point become unbound. As a result, the finer the mesh around the singular area, the larger the stress value becomes. Therefore, increasing the mesh density cannot ensure the mesh-independent and reasonable results. One method to avoid singularity is to use the model results in terms of a "calibration element" at a location close to a free edge, but distant enough to give stresses that are independent of the mesh density [18,19]. But the results are location-dependent and unable to provide a comparison analysis between different designs. Fracture mechanics approach can be applied to extract stress intensity factor or energy release rate to overcome stress singularity problem. Recently, cohesive zone model has been used for delamination problems [20,21]. However, only standard type of crack or interface crack is considered in the context of classical fracture mechanics. The singular behavior of a free edge in a bimaterial configuration is still unsolved with fracture mechanics approach.

Volume averaging, in which the stress or other parameter is averaged over an area in the vicinity of a singular point, is often used to reduce the dependency on mesh [7,8,22,23]. This approach reduces mesh sensitivity in the critical area near the singular stress field, making the analysis more meaningful. The selection of the averaging volume, however, is arbitrary in applications. For an individual solder ball, usually a very thin layer close to the interface where failure occurs over the entire interface is used for volume averaging. Some studies used a ring-shape [7,24,25], or disc-shape of volume [26,27], while other studies used the whole ball for averaging [28]. Che et al. [24–26] calculated the averaged plastic work density in both disc-shaped region and ring-shaped region at the solder-chip interface, and they found that selecting outermost ring elements as volume for averaging is desirable for fatigue life prediction. Pang et al. [27] selected both the top and bottom solder joint interface layers for volume-averaged strain energy density calculation. Zhang et al. [28] calculated the average creep strain energy density accumulation on the whole micro bump. Although many studies have been conducted on solder ball volume averaging, few studies have reported how to select volume layers for large area die attach (DA) reliability in power electronic packaging [4].

For the simplest chip on board (COB) or direct chip attach (DCA) package, it is well known that fracture begins at the corners of the die attach/die interface. However, it is still unknown which stress/strain component(s) or a combination of those components are responsible for failure. It is generally believed that inelastic strain energy plays an important role in thermal cycling conditions. However, normal stress and/or shear stress components were found to correlate better with experimental observations in some cases [6].

With the rapid development of computer-aided modeling technology, various finite element analysis software provides black-box solution strategies, allowing users to perform complete finite element analysis without knowing the details of physical settings and meshing. Using automatic meshing option and the material library provided, FEA modelers only need to provide geometry and loading conditions to arrive at the final solution. The software guide provides direct output such as von Mises stress as a basis for predicting failure.

Full detailed finite element modeling with all details of the trace structure in the substrate may be available using cluster and parallel computing. However, detailed modeling is not necessarily accompanied by increased accuracy, but by increased simulation costs and longer design cycles. Efficient finite element modeling requires proper simplification and homogenization to improve modeling and simulation efficiency.

This paper aims to provide several salient practical aspects of thermomechanical modeling in electronic packaging for building efficient and robust finite element models. It is important for engineers, especially the beginners, to have a comprehensive understanding of the general practical aspects of thermomechanical modeling. Although some concepts and practices, such as meshing and volume averaging, are known in literature, this paper provides more comprehensive and in-depth analysis and offer an ANSYS script as benchmark example in the supplemental material. Additionally, the selection of material models and the type of analysis (linear vs. nonlinear) are presented. The different output trends with different selected parameters are discussed. This paper uses a real SiC power package with a patterned substrate as a case study. Such a package is a COB or DAC type of power package that is not complex enough to obscure the important issues we intend to address. The paper is organized as follows: the geometric construction of a SiC package with a patterned substrate is described in Section 2. In Section 3, the homogenization theory, material properties, the details of finite element modeling, the averaging approach, and the loading conditions, are presented. The simulation results are presented and discussed in Section 4, and the conclusions of this work are given in Section 5.

2. The study case

The 3D view and cross-section of the SiC power package are schematically shown in Fig.1. This SiC power package consists of a copper (Cu) substrate of dimensions 20 mm by 20 mm with a thickness of 1 mm, where the die is attached to the substrate using a layer of sintered Ag with a thickness of 50 μm. A patterned layer under the die attach (DA) layer is composed of the regularly distributed Cu pillars and sintered Ag filling. In this study, the depth of the patterned layer is set as 100 μm. The cross section of the Cu pillar is set to be square, both the width and pitch of Cu pillars are 100 μm, and the boundary region of the patterned layer is designed to be filled by sintered Ag, with a width of 50 μm, as shown in Fig. 1. Here the pitch of the copper pillars is the width of sintered Ag that filled between the Cu pillars. The materials and dimensions of the chip, DA layer, substrate and the patterned layer are given in Table 1. The patterned layer with "soft" sintered Ag filling could increase the flexibility of the whole structure as thus reduce the stress, and at the same time, promoting interlocking at DA/substrate interface. However, the patterned layer makes the structure much more complex, which complicates the modeling and simulation.

3. Theory and finite element model

3.1. Equivalent properties

The complex structure of the patterned layer makes the modeling and simulation much more time-consuming. Once the patterned structure changes, the entire finite element model needs to be rebuilt. It's worth noticing that the Cu pillars are periodically and regularly embedded in sintered Ag filling (matrix), therefore, in elastic analysis, the patterned layer could be regarded as a fiber-reinforced composite that can be equivalent to a homogeneous but anisotropic layer, as shown in Fig. 2. The homogeneous equivalent layer has orthotropic properties along the longitudinal and transverse direction of the Cu pillar.

As for the orthotropic materials, nine elastic coefficients are required for the elastic analysis, namely, the longitudinal Young's modulus (E_z), transverse Young's modulus (E_x, E_y), longitudinal Poisson ratio (ν_{xz}, ν_{yz}), transverse Poisson ratio (ν_{xy}), longitudinal shear modulus (G_{xz}, G_{yz}), and the transverse shear modulus (G_{xy}) (the coordinate system is shown in Fig. 2). According to the homogenization theory of the fiber reinforced composite [29–31], the equivalent longitudinal Young's modulus of the equivalent layer (E_z) can be estimated by

$$E_z = E_{Cu}V_{Cu} + E_{Ag}(1 - V_{Cu}) \quad (1)$$

Table 1
The geometry of the SiC power package with patterned substrate.

Component	Material	Size
Die	SiC	5 mm × 1 mm × 0.1 mm
DA layer	Sintered Ag	5 mm × 1 mm × 0.05 mm
Substrate	Cu	20 mm × 20 mm × 1 mm
Patterned layer	Cu pillar and Sintered Ag filling	Depth = 0.1 mm With of Cu pillar = 0.1 mm Pitch of Cu pillar = 0.1 mm

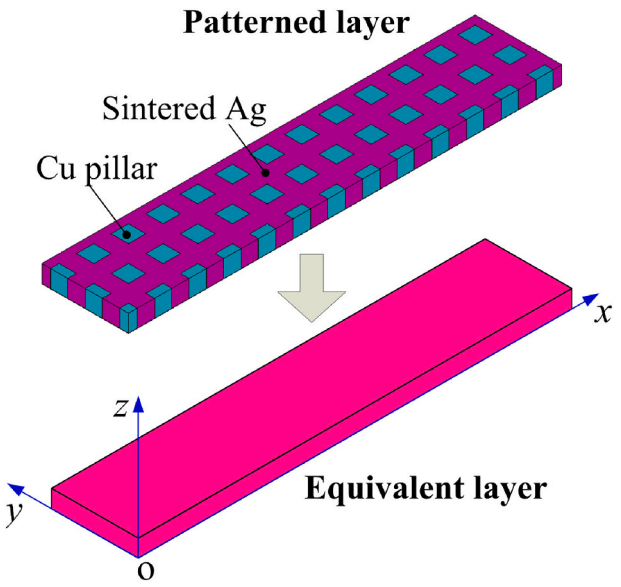

Fig. 2. The exact patterned layer and the homogeneous equivalent layer.

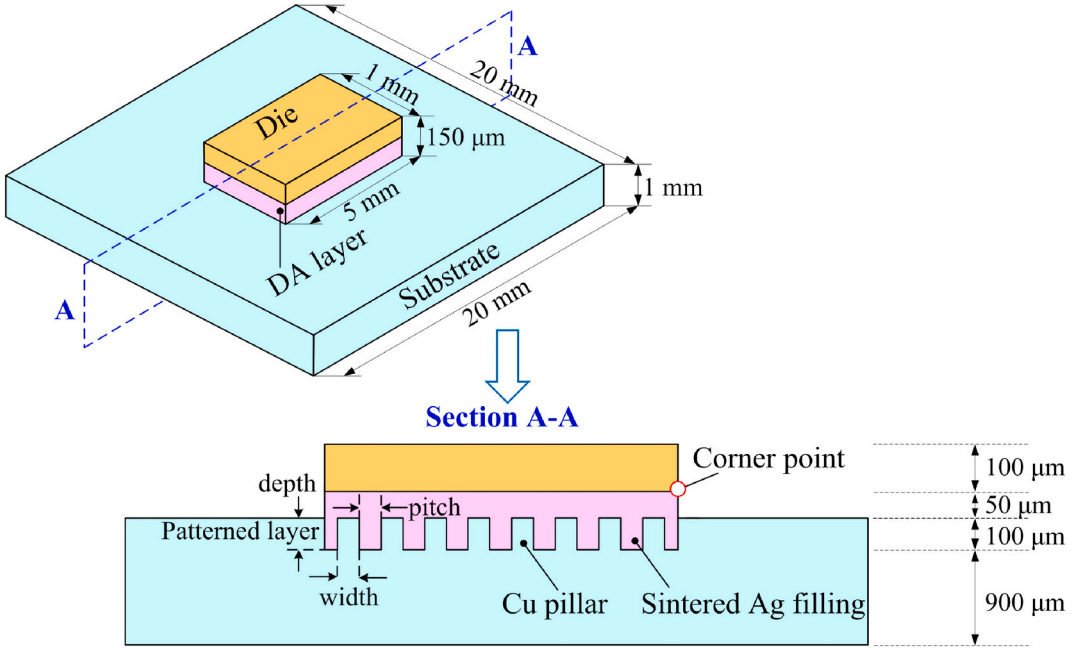

Fig. 1. The schematic diagram of the SiC power package with patterned substrate.

where E_{Cu} and E_{Ag} are elastic Young's modulus of the Cu (fiber) and sintered Ag (matrix), respectively, and V_{Cu} is the volume fraction of the Cu in the patterned layer.

And the equivalent transverse Young's modulus (E_x, E_y) are given as

$$E_x = E_y = E_{Ag}\frac{1+\xi_E\eta_E V_{Cu}}{1-\eta_E V_{Cu}} \tag{2}$$

where $\eta_E = \frac{E_{Cu}/E_{Ag}-1}{E_{Cu}/E_{Ag}+\xi_E}$, and ξ_E is geometry parameter for Young's modulus.

As for the Poisson ratio, the equivalent longitudinal ones (ν_{xz}, ν_{yz}) are

$$\nu_{xz} = \nu_{yz} = \nu_{Cu}V_{Cu} + \nu_{Ag}(1-V_{Cu}) \tag{3}$$

where ν_{Cu} and ν_{Ag} are Poisson ratio of the Cu and sintered Ag, respectively.

The equivalent transverse Poisson ratio (ν_{xy}) is

$$\nu_{xy} = \nu_{Ag}\frac{1+\xi_\nu\eta_\nu V_{Cu}}{1-\eta_\nu V_{Cu}} \tag{4}$$

where $\eta_\nu = \frac{\nu_{Cu}/\nu_{Ag}-1}{\nu_{Cu}/\nu_{Ag}+\xi_\nu}$ and ξ_ν is the geometry parameter for Poisson ratio.

For the shear modulus, the equivalent longitudinal ones (G_{xz}, G_{yz}) are given by

$$G_{xz} = G_{yz} = G_{Ag}\frac{1+\xi_G\eta_G V_{Cu}}{1-\eta_G V_{Cu}} \tag{5}$$

where $\eta_G = \frac{G_{Cu}/G_{Ag}-1}{G_{Cu}/G_{Ag}+\xi_{G1}}$ and ξ_G is the geometry parameter for shear modulus.

As for the equivalent transverse shear modulus (G_{xy}), it is calculated by

$$G_{xy} = \frac{E_x}{2(1+\nu_{xy})} \tag{6}$$

Moreover, according to the reference [32], the equivalent longitudinal CTE (a_z) of the homogenized patterned layer can be estimated by

$$a_z = \frac{a_{Cu}V_{Cu}E_{Cu} + a_{Ag}(1-V_{Cu})E_{Ag}}{V_{Cu}E_{Cu} + (1-V_{Cu})E_{Ag}} \tag{7}$$

where a_{Cu} and a_{Ag} are the CTE of the Cu and sintered Ag, respectively.

The equivalent transverse CTEs (a_x, a_y) are given by

$$a_x = a_y = V_{Cu}(1+\nu_{Cu})a_{Cu} + (1-V_{Cu})(1+\nu_{Ag})a_{Ag} - a_z\nu_{xz} \tag{8}$$

There are nine elastic constants (E_x, E_y, E_z, ν_{xy}, ν_{xz}, ν_{yz}, G_{xz}, G_{yz}, G_{xy}) and three thermal parameters (a_x, a_y, a_z) of the orthotropic material, which are determined by twelve parameters, including six elastic constants (E_{Cu},E_{Ag}, ν_{Cu}, ν_{Ag}, G_{Cu}, G_{Ag}), two thermal properties (a_{Cu}, a_{Ag}), three shape parameters (ξ_E, ξ_ν, ξ_G), and one volume fraction parameter (ν_{Cu}). Since the copper pillar has a square section, the geometry parameters ξ_E, ξ_ν, and ξ_G are approximately set as 2.0, 2.0 and 1.0, respectively. The equations to calculate the shape parameters in other cases can be found in reference [29, 33].

It should be pointed out that, there are indeed only five independent elastic constants for the equivalent homogeneous layer, that is, the equivalent longitudinal Young's modulus (E_z), the equivalent transverse Young's modulus ($E_x = E_y$), the equivalent longitudinal Poisson ratio ($\nu_{xz} = \nu_{yz}$), the equivalent transverse Poisson ratio (ν_{xy}), and the equivalent longitudinal shear modulus ($G_{xz} = G_{yz}$). These five elastic constants are determined by five parameters, i.e., the volume fraction of Cu (V_{Cu}), and the four independent elastic constants of Cu and sintered Ag (E_{Cu}, E_{Ag}, ν_{Cu}, ν_{Ag}). Among these parameters, the volume fraction of the Cu (V_{Cu}) depends on the dimensions of the Cu pillar's width and pitch. For different V_{Cu}, the equivalent thermomechanical properties of the homogenized patterned layer (equivalent layer) can be calculated.

The material properties of the SiC device used for simulation in linear elastic analysis are listed in Table 2 [34,35], and the equivalent mechanical and thermal properties of the homogenized patterned layer are calculated by the Eqs. (1)–(8), which are given in Table 3. The homogeneous layer shows the modulus (E_z) of about 30% of the Cu's modulus, but about 4.7 times of sintered Ag's modulus.

Table 2
Material properties of the SiC device [34,35].

Material	Young's modulus (GPa)	Poisson ratio	CTE (m/ °C)
SiC	501	0.45	3.4×10^{-6}
Sintered Ag	7	0.37	2.0×10^{-5}
Cu	110	0.35	1.7×10^{-5}

3.2. Mesh

The finite element software ANSYS Mechanical APDL (version 19.0) was used. A quarter-symmetric 3D model is adopted due to the symmetry. Multizone technique is applied during meshing, and the hexahedral mapped mesh is used for the entire model. By doing so the shape and size of the elements can be well controlled, and all elements are cuboid or cube with 20 nodes.

The failure mainly occurs at the corners of the interface between the die and DA layer (see Fig. 1) in a typical COB or DAC package [4,5], thus, the region near the corner point at DA/die interface is taken as the critical location. The finite element analyses are focusing on the thermomechanical behavior of the DA layer near the corner point. To achieve reliable and meaningful results, the elements near the edge of the DA layer are refined, and the element at the corner point of the DA layer is fixed as 5 μm × 5 μm × 5 μm in all simulations, as shown in Fig. 3. In parametric analysis, the APDL script is designed to fix the size of the element at the corner to have a meaningful comparison of stresses, despite the stress singularity at the interface edge.

Fig. 4a gives the exact finite element model with patterned substrate details, while Fig. 4b is a simplified finite element model with homogeneous equivalent layer (equivalent finite element model). The exact finite element model serves for the purpose to validate the equivalent model in linear analysis, as well as to investigate the thermomechanical behavior in nonlinear analysis. It should be pointed out that the equivalent model is only applicable for the linear elastic analysis. When the viscoplastic behavior is considered the homogenization theory is inapplicable, and the exact finite element model with the patterned substrate details is required.

3.3. Stress-strain relationship of sintered Ag

In Section 3.1, the linear elastic material properties of sintered Ag are provided. When the nonlinear plastic deformation and rate-dependent behavior of the bonded material are considered, different nonlinear material models for stress-strain relationship can be used. The Anand model has been widely used in the electronic packaging industry for solder materials to account for both the rate-dependent (creep) and rate-independent (plasticity) deformation nature [36]. In this study, the Anand model parameters of sintered Ag, given by reference [37], are used and listed in Table 4. There are nine material constants in Anand model. Since this is a rate form of the stress-strain relationship, the simulation will require the time duration under the given loading condition. In the present study, however, the effect of inertia is neglected. The problem is quasi-static.

3.4. Stress singularity and volume averaging

For structures containing either dissimilar materials, or cracking and delamination, the stresses are singular at the corners of geometric shape, the edge of the interface between dissimilar materials, and the tip of the interface crack (or delamination) [5,9,38]. In reference [9], stress singularities arising in bimaterial configurations are grouped into three

Table 3
Equivalent mechanical and thermal properties of the homogenized patterned layer.

Mechanical properties	Equivalent Young's modulus (GPa)		Equivalent Poisson ratio		Equivalent shear modulus (GPa)		Equivalent CTE (m/°C)	
Symbol	E_z	E_x, E_y	ν_{zx}, ν_{yz}	ν_{xy}	G_{zx}, G_{yz}	G_{xy}	a_z	a_x, a_y
Value	32.75	12.50	0.365	0.365	7.49	4.58	1.75×10^{-5}	1.99×10^{-5}

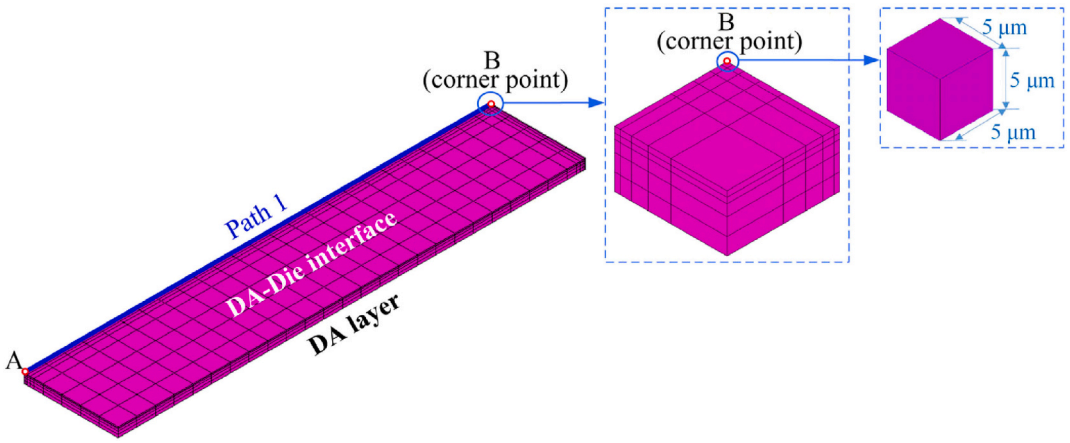

Fig. 3. The details of the mesh structure of the DA layer and corner region.

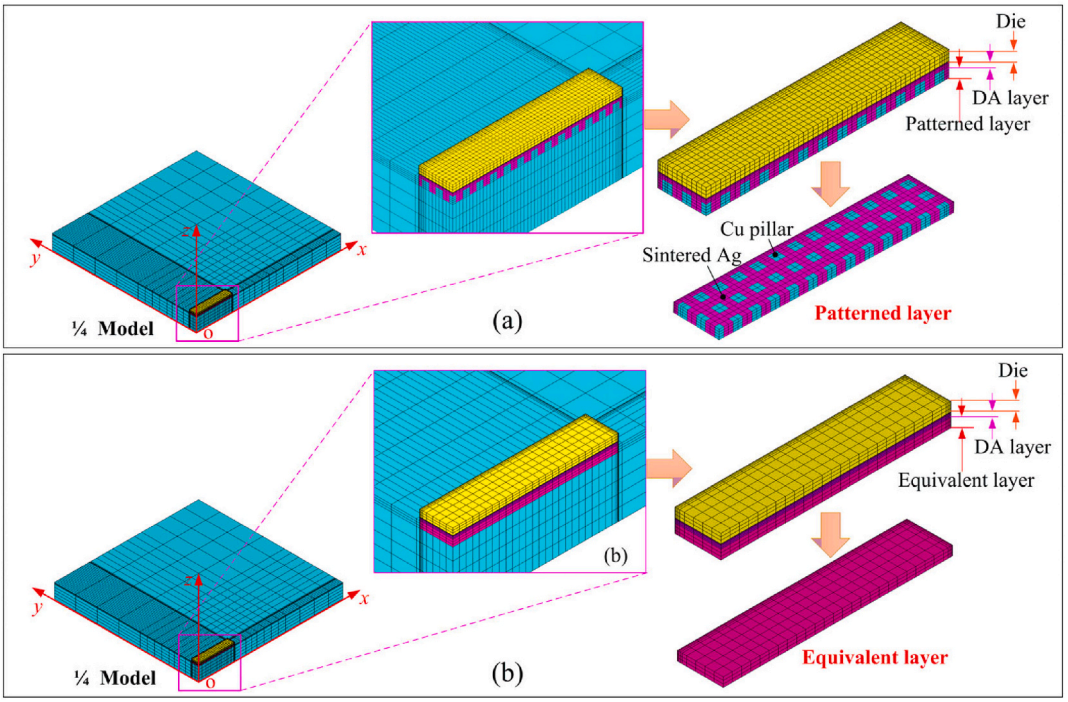

Fig. 4. The finite element model of the SiC device (1/4 model): (a) exact finite element model with patterned substrate details, (b) equivalent finite element model.

general cases: 1) angular corner of a homogeneous material; 2) angular corner of bimaterial wedge; and 3) bimaterial wedge with adhesion. Free-edge of a bonded dissimilar material is a special case for the second category. In general, fracture mechanics approaches are needed for the extraction of meaningful fracture parameters, such as stress intensity factor or energy release rate. Recently, cohesive zone model has been used for delamination problems [20,21]. However, only standard type of crack or interface crack is considered in the context of classical fracture mechanics. The singular behavior of a free edge in a bimaterial configuration is still unsolved with fracture mechanics approach.

As a general practice for convenience, stresses at the corner points can still be used for a relative comparison among design cases. To obtain meaningful stress results, the size and shape of the element around the corner points must be fixed, as shown in Fig. 3. In this way, the output of stresses from finite element analysis is an average quantity over the element volume, and the value of stress will be loosely less dependent on the mesh when other design parameters change. In elastic analysis, the average stress solution in the element where the vertex node is located (element solution), rather than the node solution at the vertex is used. However, the value of stress will change significantly with the element

Table 4
Anand model parameter for sintered Ag [37].

Parameter	Symbol	Value
Pre-exponential factor	A (s^{-1})	9.81
Activation energy/universal gas constant	A/R (°K)	5706
Multiplier of stress	ξ	11
Strain rate sensitivity of stress	m	0.66
Coefficient for deformation resistance saturation	s (MPa)	67.3
Deformation resistance	n	0.00326
Hardening/softening constant	h_o (MPa)	1.58×10^4
Strain rate sensitivity of hardening or softening	a	1
Initial deformation resistance	s_o (MPa)	2.77

size due to singularity. The absolute value of stresses at the singular points has no actual meanings.

To further reduce the mesh dependency, the volume averaging method is usually adopted. The volume averaging method has been particularly used in the nonlinear plastic analysis to achieve mesh-independent plastic work density (denoted by PLWK in ANSYS). In nonlinear viscoplastic analysis, the fatigue is closely related to the PLWK per cycle [6–8,39]. The PLWK at a particular node is defined as the time integral of the product of stresses and incremental strains in all six directions at that node. The average PLWK accumulated in a fixed volume is defined as:

$$\Delta W_{ave} = \frac{\Sigma \Delta W_i V_i}{V} \tag{9}$$

where ΔW_i is PLWK accumulated per cycle for the i-th element, V_i is the volume of the i-th element, and $V = \Sigma V_i$ is the total volume of a defined fixed volume. Despite many studies on solder ball volume averaging, few studies reported how to select a volume layer for a large-area die-attach in a power electronics package [4]. In this work, the average PLWK accumulated per cycle is calculated based on a thin and small square layer near the critical location during thermal cycling. Fig. 5 shows the thin square layer that is selected as the region of interest, the dimension of which is 50 μm × 50 μm with a depth of 5 μm.

3.5. Loading conditions

Symmetrical condition is applied on the middle planes of the 1/4 finite element model (see planes *xoz* and *yoz* in Fig.4). In addition, all directions of the point node at center only in the backside of the Cu substrate is constrained to prevent rigid body motion.

Uniform temperature is loaded on the entire model. If we consider the failure caused by the temperature rise or cooling in a single loading condition, the solidus temperature of solder material should be used [7]. If we are concerned with the thermomechanical behavior caused by thermal cycling, T_{max}, the high dwell temperature of thermal cycle, is recommended as the initial stress-free temperature. Taking the thermal cycling profile illustrated in Fig.6 for example, stress free temperature is set as 150 °C. In addition, each cycle includes four periods: temperature ramp down from 150 °C to −65 °C in the first 900 s; temperature dwelling at −65 °C in the second 900 s; temperature ramp up linearly from −65 °C to 150 °C in the third 900 s; and the temperature dwelling at 150 °C in the last 900 s of one cycle. For each load step of a thermal cycle, sufficient sub-time-steps are needed to achieve a smooth convergence of the solution [40].

4. Results and discussions

4.1. Accuracy of the equivalent model

Fig. 7 gives the Mises stress, normal stress and shear stress (τ_{xz}) counter maps of the DA/die interface at −65 °C. The maximum Mises stress, normal stress and shear stress are located at the corner point for both the exact full model and equivalent model. The stresses distribution obtained by the equivalent model matches well with the exact full model, though the stresses of the exact full model distributes some more irregularly due to the existence of the patterned layer.

Fig. 8 further gives the distributions of the von Mises stress, shear stress and normal stress from point A to point B along the Path 1 (see

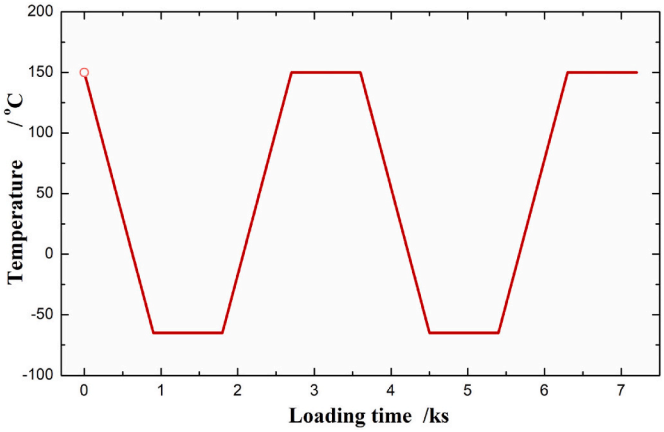

Fig. 6. Thermal cycling profile used in this study. The highest and lowest temperatures are 150 °C and − 65 °C, respectively, each cycle lasts 3600 s and both the dwell and ramp time are 900 s.

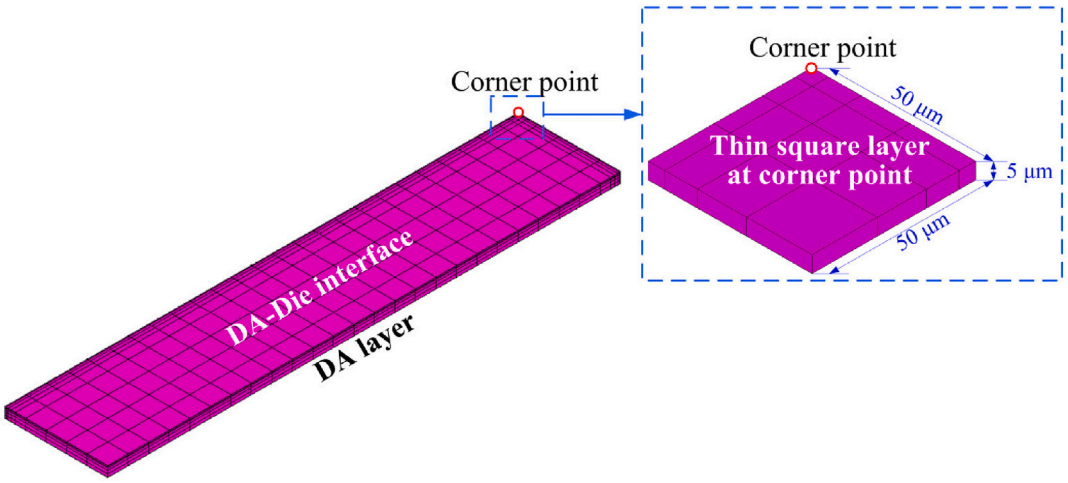

Fig. 5. The thin square layer used for the definition of the average PLWK.

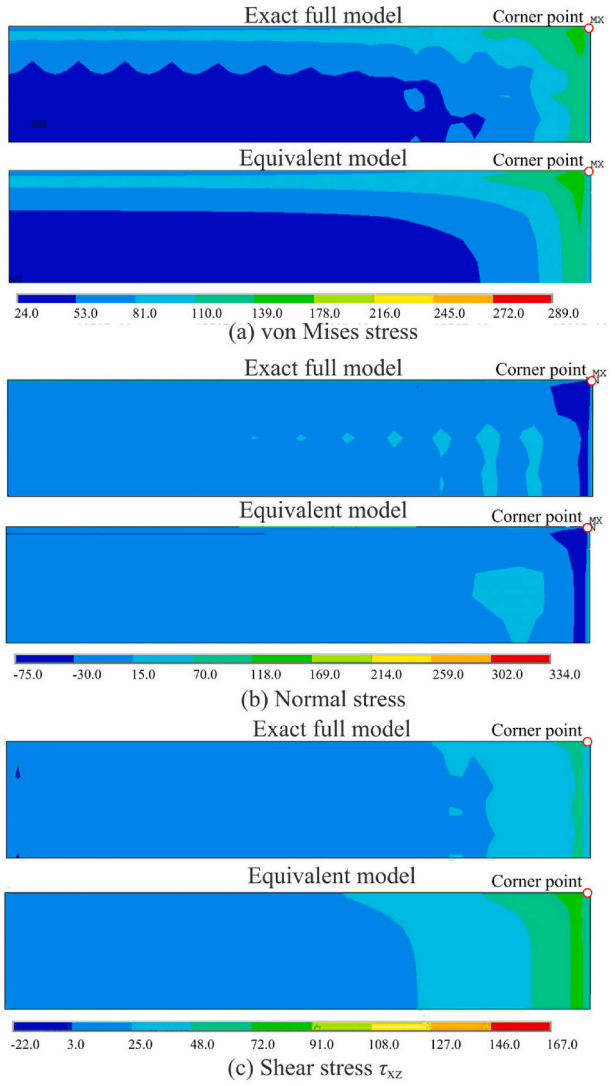

Fig. 7. Stresses map at DA/die interface at −65 °C in linear elastic analysis.

Fig. 3). It can be noted that the distributions of each stress component obtained from the equivalent model are in good agreement with those obtained from the exact full model. Fig. 8 also shows that there exists stress singularity at the corner point, which indicates that the finer mesh gives rise to larger stress value. Therefore, it is important to fix the size of the element at the corner point for a relative comparison among design cases. In this work, the size of the element at the corner point is fixed as 5 μm × 5 μm × 5 μm in all cases to eliminate the size effect caused by singularity. This approach is different from the "calibration element" concept [18,19] as stresses at corner location can capture the relative intensity of stress value in an average sense at singular point.

Fig. 9 shows the evolutions of the von Mises stress, shear stress and normal stress at the corner element obtained from the equivalent model and exact model. Again, the equivalent model presents an excellent accuracy compared to the results from the exact model. It can be seen from Fig.9 that the elastic stresses increase linearly with decreasing the temperature. They reach their maximum values as the temperature reduces to the lowest value at 900 s. The stresses maintain at the highest values until the temperature becomes to increase at 1800 s, and then reduce to zero when the temperature rises to 150 °C at 2700 s. Then the second cycle begins, which is the same as the first cycle because of the linear elastic nature.

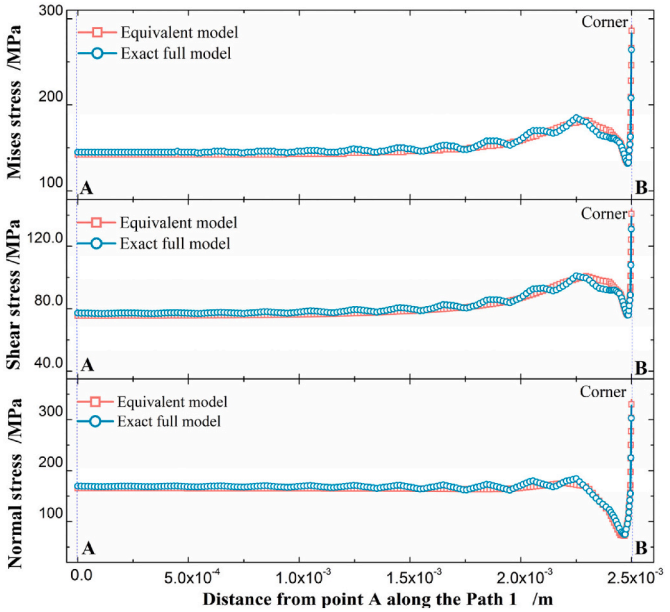

Fig. 8. Distributions of Mises stress, shear stress and normal stress along the Path 1 (define in Fig. 3).

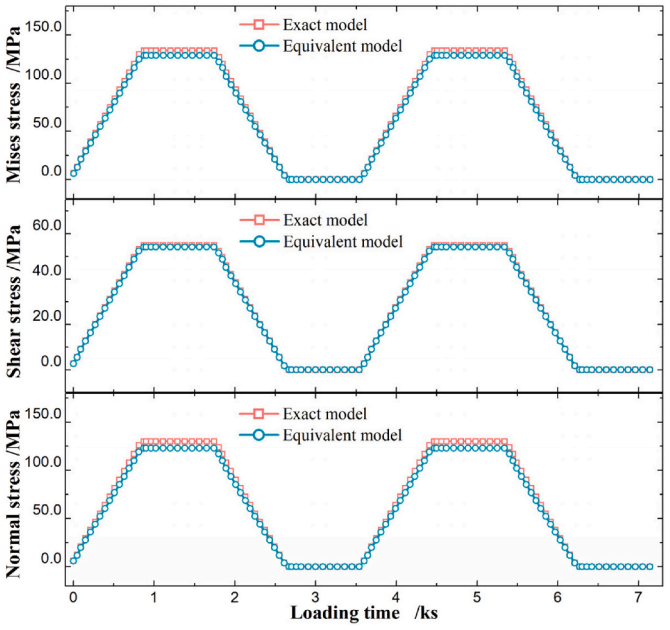

Fig. 9. Comparison of the stress evolution between the exact full model and equivalent model.

4.2. Mesh dependence

The element size at the corner point is fixed as 5 μm × 5 μm × 5 μm in above mentioned results. To investigate the mesh dependency, Fig. 10 shows the stresses at the corner for different mesh sizes obtained in elastic analysis. As expected, the values of the maximum stresses have great dependency on the mesh size. It is hard to achieve a stable value by decreasing the mesh size due to the stress singularity. Stresses increase rapidly with decreasing the mesh size even when the mesh size is smaller than 2.5 μm. This is in accordance with the fact that both shear and normal stresses present singularity at the corner [14,15].

Fig. 11 plots the stresses at the corner point when Anand model is applied for sintered Ag. With reducing the mesh size, the von Mises

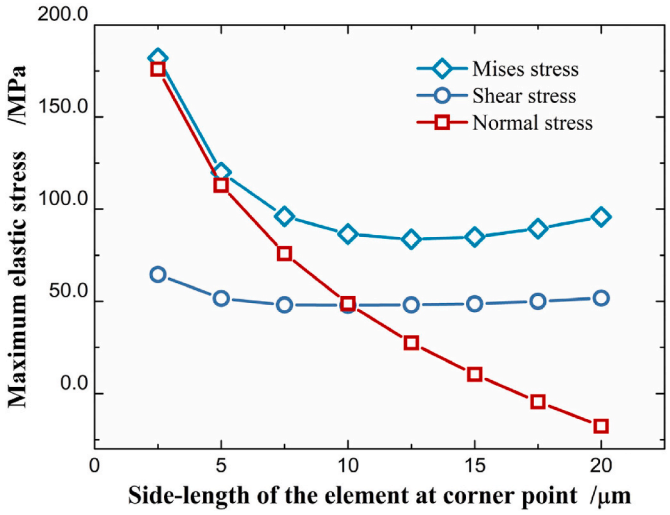

Fig. 10. Stresses vs. mesh size at corner in linear elastic analysis.

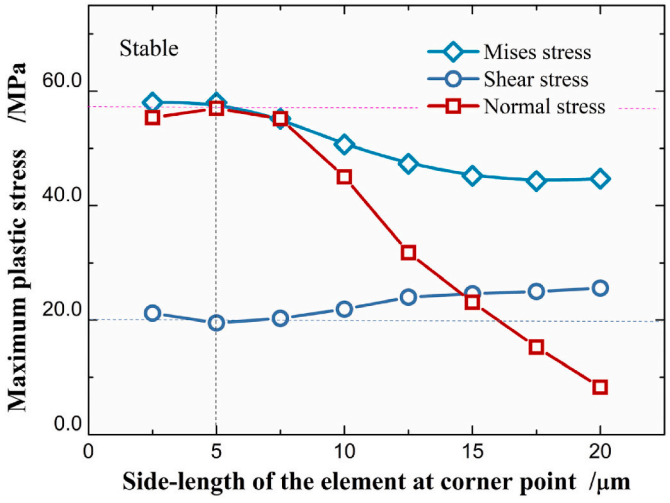

Fig. 11. Stresses vs. mesh size at corner point in nonlinear plastic analysis.

stress and normal stress increase while the shear stress decreases. Shear stress maintains a relative stable value in both elastic and plastic analysis, and the normal stress changes more significantly. When the mesh size is smaller than 5 μm the results are stabilized. It is also worth pointing that when a larger mesh size is used at the corner, the normal stress approaches to zero in nonlinear plastic analysis, but normal stress becomes compressive in linear elastic analysis (see Fig. 10).

4.3. *Effect of stress-strain model*

To illustrate the impact of material model on simulation results, we consider 3 design cases: the one without patterned substrate (case 1), the one with patterned substrate but without gap (case 2), and the one with both patterned substrate and gap (case 3), as shown in Fig. 12. When the gap is applied, the depth and width of the gap is set as 100 μm and 50 μm, respectively. Fig. 13 gives the stress evolution results based on linear elastic analysis. For the case with patterned substrate but without gap (case 2), the stresses (von Mises, normal and shear) are increasing compared with the traditional design (case 1). When the gap is applied (case 3), all stresses decrease. This is because that the constraint by the substrate on the patterned and DA layers is reduced by "soft" gap so that the patterned layer and DA layer can deform more freely. Therefore the stresses are reduced.

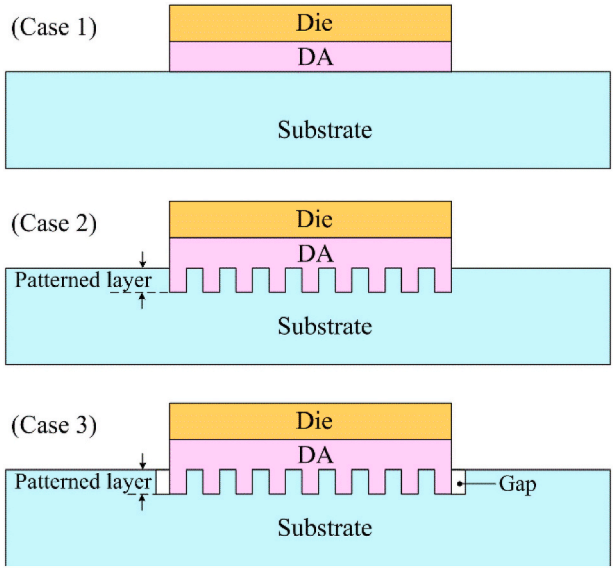

Fig. 12. Three design cases of the SiC power package.

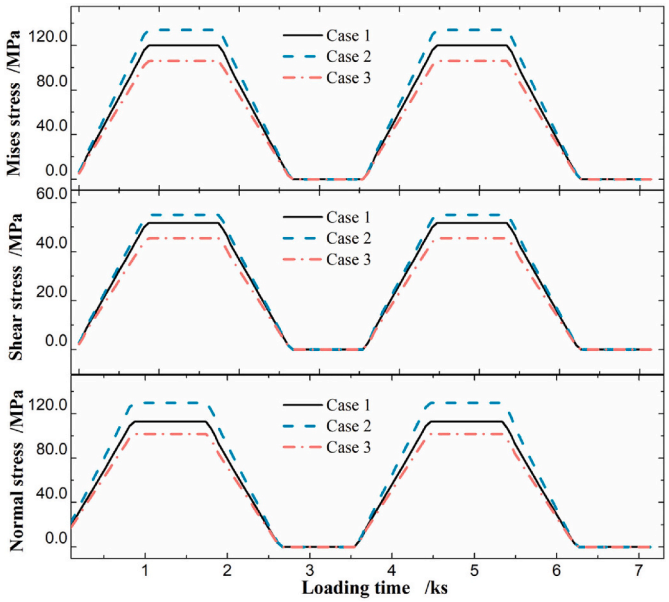

Fig. 13. Stress evolution of the three design cases obtained by linear elastic analysis.

However, for a viscoplastic analysis using Anand model, the patterned substrate with or without gap almost does not affect the DA/die corner stress, as shown in Fig. 14. Viscoplastic analysis presents completely different results from the linear elastic analysis. The underlying mechanism is that in an elastic analysis, the stresses vary linearly with the deformation, therefore stresses change significantly when the gap is applied. However, in viscoelastic analysis, the stresses are already released by the viscoelastic deformation inside DA layer, and thus the stresses change a little with the presence of the gap. The results indicate that the nonlinear analysis presented completely different trend results.

Moreover, the evolution of the viscoplastic stresses also shows a completely different trend compared with the linear elastic analysis. In the nonlinear viscoplastic analysis, the stress changes with the temperature nonlinearly, it varies even during the dwelling stage. The stresses reach their maximum values when the temperature drops to the lowest point, but do not return to zero when the temperature returns to the

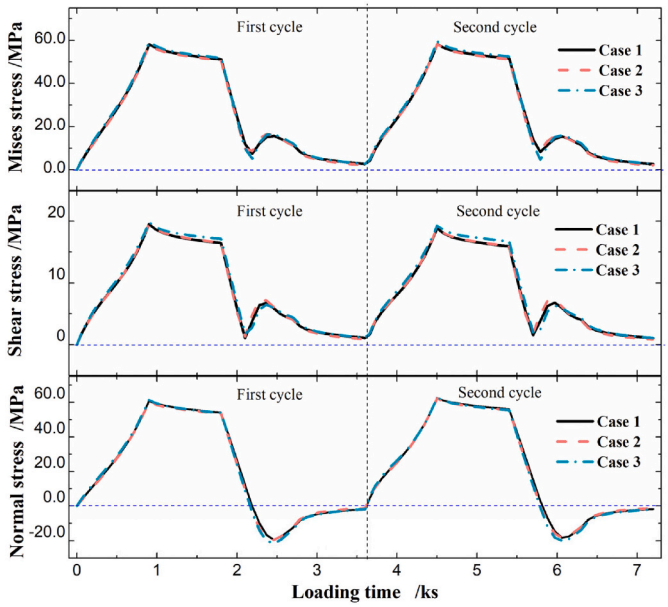

Fig. 14. Stress evolution of the three design cases obtained by nonlinear viscoplastic analysis.

initial value. This indicates residual stress occurs after unloading.

In the nonlinear plastic analysis, there are some differences of the evolution tendency between the normal stress and shear stress. The shear stress is always positive, but there exists a tensile-compressive transition of the normal stress during the heating stage (1800 s–2700 s). Both the shear stress and normal stress do not return to zero when the temperature returns to the initial value (150 °C). The negative residual normal stress hinders fracture opening and is beneficial for retarding the fatigue fracture [6].

Fig. 15 further gives the average PLWK per cycle for these 3 cases. The patterned substrate without gap does not affect the average PLWK. But when the gap is applied, the average PLWK decreases slightly.

4.4. Volume averaging

In nonlinear viscoplastic analysis, the fatigue failure becomes the most important issue [5,40]. The fatigue failure due to temperature cycling in DA is closely related to the PLWK per cycle, as defined in Eq. (9). The maximum value of the PLWK per cycle is found to be at the corner regions, which depends on the particular mesh used in the finite element model. Fig.16 gives the PLWK per cycle at the corner point accumulated in the second cycle for different element sizes, together with the average PLWK per cycle in the thin square layer using Eq. (9). It shows evident dependence of the PLWK on the element size at the corner point. When the element size at the corner point increases from 5 μm to 15 μm, the PLWK accumulated in second cycle decreases from 1.85 MJ/m^3 to 0.73 MJ/m^3 by 60.5%. On the other hand, when the volume averaging method is applied, the averaged PLWK is almost independent on the mesh size, the value of which stabilizes at about 0.56 MJ/m^3. Fig. 17 shows the mesh details of the three different meshes in the thin square layer, which give the same results of the averaged PLWK per cycle. This shows clearly that the mesh size dependence can be effectively eliminated with the volume averaging method. The volume averaging is usually established in solder ball fatigue analysis, and the ring-shape, disc-shape, and even the whole solder ball are usually adopted as the averaging volume [24–28]. In this work, the accumulated PLWK is averaged in a thin and small square layer on the DA interface.

As the averaged PLWK per cycle may be different in each cycle, the selection of initial stress-free temperature is important. There has been a long-running debate on the selection of initial stress-free temperature in temperature cycle modeling. There are three most commonly used initial stress-free temperatures [6]. One is the solidus temperature of solder alloy (e.g. 217 °C for SnAgCu). This condition considers that the solder joints start to provide mechanical support as soon as the solder material solidifies during the reflow process. The second one is the room temperature as the initial stress-free condition (e.g. 25 °C). This assumes that the shipping and storage time is sufficient to relax all the residual stresses in solder joints from the assembly process. The last one uses the high dwell temperature of thermal cycle or operating conditions (denoted as T_{max}, e.g. = 150 °C for thermal cycling from to −65 °C 150 °C). This assumes that after several thermal cycles, the package reaches a stabilized cyclic pattern where the lowest stresses are seen at the end of the high temperature dwell period. The previous study has shown that setting T_{max} as the initial stress-free temperature will achieve stabilized solution quickly and thus, to significantly increase the computational efficiency. Fig. 18 plots the averaged PLWK per cycle in the first 10 cycles in the present study. It shows that the PLWK per cycles stabilizes in the second cycle.

In this paper, we presented several stress components and PLWK. It has been unknown which parameter, such as, normal stress component, shear stress component, or a combined equivalent stress indicator (like

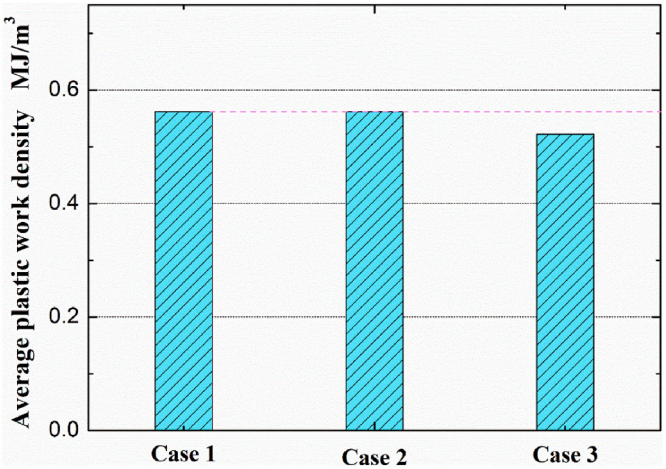

Fig. 15. The average PLWK of the thin square layer per cycle for the three cases.

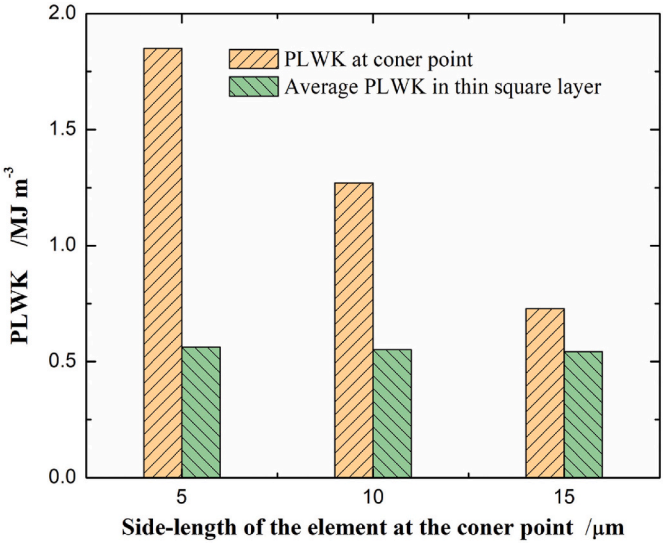

Fig. 16. The PLWK at corner point and the average PLWK of the thin square layer in second cycle.

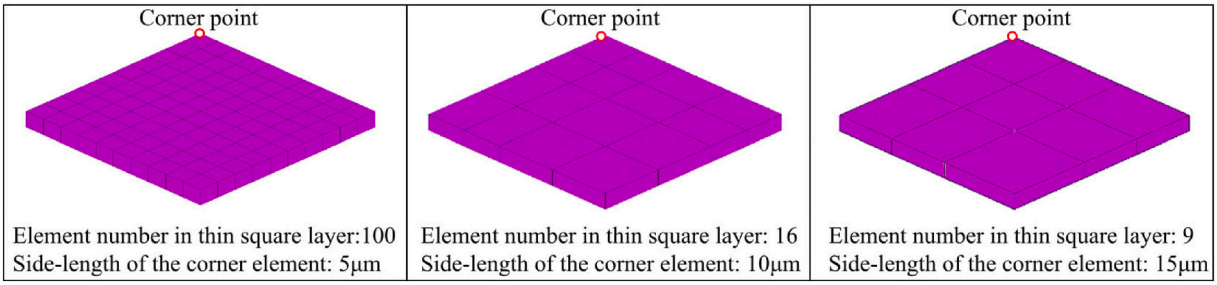

Fig. 17. Mesh details of three different meshes in the thin square layer.

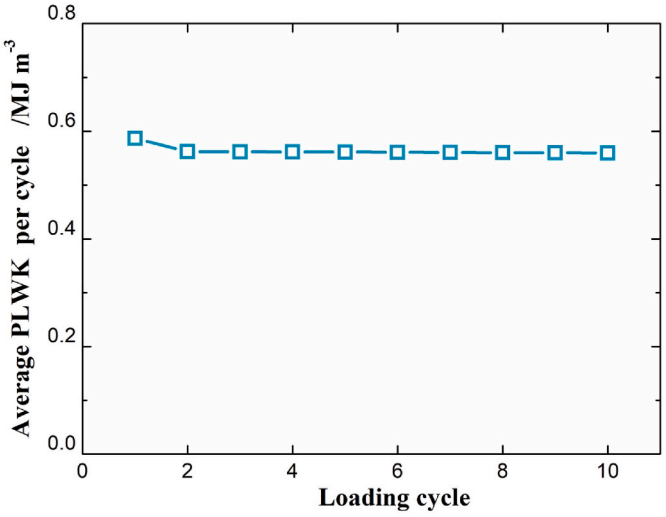

Fig. 18. Average PLWK per cycle vs. loading cycle.

von Mises stress), or strain energy density, is to be used to correlate with experimental data. Although it is generally recognized that in terms of fatigue failure, inelastic energy density plays an important role, we have observed that other parameters, such as stresses, need to be considered too [6]. There is no single parameter that can fit all scenarios, even with the well-known failure locations and mechanisms from experiment.

5. Conclusions

In this work, some essential problems of thermomechanical modeling of electronics packaging were discussed based on the studies of a SiC power package with patterned substrate layer. Both the elastic and viscoplastic behaviors were analyzed. The main conclusions are as follows:

1. A homogenization-based equivalent model is introduced to simplify the finite element models. The equivalent model presents the excellent agreement with the exact finite element model solutions. Such an approach can be effectively used in elastic stress analysis for the electronic packages with periodically distributed substructures.
2. Stresses singularity takes place at the free edge of bimaterial interface, the absolute value of the stress components from finite element analysis has no actual meaning. As a general practice for convenience, stresses at the singular points can still be used for a relative comparison among design cases, but the size and shape of the element around the corner points must be fixed.
3. To further eliminate the mesh effect, the volume averaging method can be used. In this work, a thin square layer on the DA interface is selected for local volume averaging. With using the presented volume averaging method, the mesh size dependence can be effectively eliminated for large-area die attach problems.
4. We presented a case study using both linear and nonlinear elastic analysis, and in some cases, different trend results were obtained between linear and nonlinear analysis. This implies that the choice of analysis type and material model are important to reflect the actual behavior. Although linear elastic analysis provides good estimate as preliminary results, it must be noted that the opposite trend could occur in some cases when nonlinear analysis is applied.
5. We presented the results of several stress components and the inelastic strain energy density. Different output parameters may lead to different conclusions. The appropriate use of material models and the correct selection of the output metric should be based on the experimental data and failure mechanisms.

CRediT authorship contribution statement

Guigen Ye: Methodology, Software, Writing – original draft. **Xuejun Fan:** Conceptualization, Validation, Writing – review & editing. **Guoqi Zhang:** Conceptualization, Supervision.

Declaration of competing interest

We declare that we have no financial and personal relationships with other people or organizations that can inappropriately influence our work, there is no professional or other personal interest of any nature or kind in any product, service and/or company that could be construed as influencing the position presented in, or the review of, the manuscript entitled “Thermomechanical Modeling of a SiC Power Package in Heterogeneous Integration System”.

Acknowledgements

The authors would like to acknowledge A. M. Gheytaghi and the Chip Integration Technology Center (CITC) for many valuable discussions and suggestions.

Appendix A. Supplementary data

Supplementary data to this article can be found online at https://doi.org/10.1016/j.microrel.2022.114514.

References

[1] J.M. Nassar, G.A.T. Sevilla, S.J. Velling, M.D. Cordero, M.M. Hussain, A CMOS-compatible large-scale monolithic integration of heterogeneous multi-sensors on flexible silicon for IoT applications, in: International Electron Devices Meeting (IEDM), 2016 (pp. 18.6.1-18.6.4).
[2] P.V.K. Nittala, P. Sen, Scaling a fluorescent detection system by polymer assisted 3d integration of heterogeneous dies, IEEE J. Micro Electromech. Syst. 27 (2018) 896–909.
[3] P.V.K. Nittala, K. Haridas, S. Nigam, S. Tasneem, P. Sen, Characterization and optimization of bonding and interconnect technology for 3d stacking of ultra-thin dies, J. Vac. Sci. Technol. B 39 (2021), 052207.

[4] Y. Liu, Power Electronic Packaging - Design, Assembly Process, Reliability and Modeling. Springer Verlag, New York, 2012.
[5] G.Q. Zhang, W.D. van Driel, X.J. Fan, Mechanics of Microelectronics, Springer, 2006.
[6] P.K. Bhatti, M. Pei, X.J. Fan, Reliability analysis of SnPb and SnAgCu solder joints in FC-BGA packages with thermal enabling preload, in: Proceedings of Electronic Components and Technology Conference (ECTC), 2006, pp. 601–606.
[7] X.J. Fan, M. Pei, P.K. Bhatti, Effect of finite element modeling techniques on solder joint fatigue life prediction of flip-chip BGA packages, in: Proceedings of Electronic Components and Technology Conference (ECTC), 2006, pp. 972–980.
[8] X.J. Fan, B. Varia, Q. Han, Design and optimization of thermo-mechanical reliability in wafer level packaging, Microelectron. Reliab. 50 (2010) 536–546.
[9] X.J. Fan, H.B. Wang, T.B. Lim, Investigation of the underfill delamination and cracking for flip chip modules under temperature cyclic loading, in: IEEE Transactions on Components, Manufacturing and Packaging Technologies vol. 24, 2001, pp. 84–91.
[10] L. Chen, T.F. Jiang, X.J. Fan, Die and package level thermal and thermal/moisture stresses in 3-d packaging: modeling and characterization, in: Li Yan, Goyal Deepak (Eds.), 3D Microelectronic Packaging: From Fundamentals to Applications, 2nd edition, Springer, 2020, pp. 431–469.
[11] M. Ciappa, Selected failure mechanisms of modern power modules, Microelectron. Reliab. 42 (2002) 653–667.
[12] Z. Wang, G. Ye, X. Li, S. Xue, L. Gong, Thermal-mechanical performance analysis and structure optimization of the TSV in 3D IC, IEEE Trans. Compon. Packag. Manuf. Technol. 11 (2021) 822–831.
[13] L. Guo, J. Xiang, J.P. Latham, B. Izzuddin, A numerical investigation of mesh sensitivity for a new three-dimensional fracture model within the combined finite-discrete element method, Eng. Fract. Mech. 151 (2016) 70–91.
[14] E. Suhir, Analysis of interfacial thermal stresses in a trimaterial assembly, J. Appl. Phys. 89 (2001) 3685–3694.
[15] M.Y. Tsai, C.H. Hsu, C.N. Han, A note on Suhir's solution of thermal stresses for a die-substrate assembly, J. Electron. Packag. 126 (2004) 115–119.
[16] H.R. Ghorbani, J.K. Spelt, Analytical elasto-creep model of interfacial thermal stress and strains in trilayer assemblies, Int. J. Solids Struct. 43 (2006) 7424–7449.
[17] C. Basaran, Y. Zhao, Mesh sensitivity and FEA for multi-layered electronic packaging, J. Electron. Packag. 123 (2001) 218–224.
[18] D.R. Shirley, H.R. Ghorbani, J.K. Spelt, Effect of primary creep and plasticity in the modeling of thermal fatigue of SnPb and SnAgCu solder joints, Microelectron. Reliab. 48 (2008) 455–470.
[19] C. Selvanayagam, X. Zhang, R. Rajoo, D. Pinjala, Modeling stress in silicon with TSVs and its effect on mobility, IEEE Trans. Compon. Packag. Manuf. Technol. 1 (2011) 1328–1335.
[20] M. Elices, G.V. Guinea, J. Gómez, J. Planas, The cohesive zone model: advantages, limitations and challenges, Eng. Fract. Mech. 69 (2002) 137–163.
[21] Z.H. Jin, C.T. Sun, Cohesive zone modeling of interface fracture in elastic bi-materials, Eng. Fract. Mech. 72 (2005) 1805–1817.
[22] A. Syed, Accumulated creep strain and energy density based thermal fatigue life prediction models for SnAgCu solder joints, in: 54th Electronic Compnents and Technology Conference, 2004, pp. 737–746.
[23] R. Darveaux, Effect of simulation methodology on solder joint crack growth correlation and fatigue life predection, J. Electron. Packag. 124 (2002) 147–154.
[24] F.X. Che, J.H.L. Pang, Vibration reliability test and finite element analysis for flip chip solder joints, Microelectron. Reliab. 49 (2009) 754–760.
[25] F.X. Che, J.H.L. Pang, Fatigue reliability analysis of Sn–Ag–Cu solder joints subject to thermal cycling, IEEE Trans. Device Mater. Reliab. 13 (2012) 36–49.
[26] F.X. Che, Study on board level solder joint reliability for extreme large fan-out WLP under temperature cycling, in: IEEE 18th Electronics Packaging Technology Conference (EPTC), 2016, pp. 207–212.
[27] H.L.J. Pang, F.X. Che, W.H. Zhu, S. Wei, A.Y.S. Sun, Modeling constitutive model effect on reliability of lead-free solder joints, in: 7th International Conference on Electronic Packaging Technology, 2006, pp. 1–6.
[28] X. Zhang, F.X. Che, J.K. Lin, Reliability study of 3D IC packaging based on through-silicon interposer (TSI) and silicon-less interconnection technology (SLIT) using finite element analysis, Microelectron. Reliab. 61 (2016) 64–70.
[29] J.C. Halpin, J.L. Kardos, The Halpin-Tsai equations: a review, Polym. Eng. Sci. 16 (1976) 344–352.
[30] J.C. Halpin, Stiffness and expansion estimates for oriented short fiber composites, J. Compos. Mater. 3 (1969) 732–734.
[31] R. Hill, Theory of mechanical properties of fiber-strenthened materials: I Elastic behavior, J. Mech. Phys. Solid 12 (1964) 199–212.
[32] R.A. Schapery, Thermal expansion coefficients of composite materials based on energy principles, J. Compos. Mater. 2 (1968) 380–384.
[33] S. Zhao, Z. Zhao, Z. Yang, L.L. Ked, S. Kitipornchaia, J. Yang, Functionally graded graphene reinforced composite structures: a review, Eng. Struct. 210 (2020), 110339.
[34] K.S. Siow, Die-Attach Materials for High Temperature Applications in Microelectronics Packaging, Springer, Cham, 2019.
[35] B. Hu, J.O. Gonzalez, L. Ran, H. Ren, Z. Zeng, W. Lai, B. Gao, O. Alatise, H. Lu, C. Bailey, P. Mawby, Failure and reliability analysis of a SiC power module based on stress comparison to a Si device, IEEE Trans. Device Mater. Reliab. 17 (2017) 727–737.
[36] L. Anand, Constitutive equations for hot working of metals, Int. J. Plast. 29 (1985) 213–231.
[37] D. Yu, X. Chen, G. Chen, G.Q. Lu, Z.Q. Wang, Applying Anand model to low-temperature sintered nanoscale silver paste chip attachment, Mater. Des. 30 (2009) 4574–4579.
[38] M. Prukvilarilert, H. Koguchi, Stress singularity analysis around the singular.
[39] W. Lee, L. Nguyen, G. Selvaduray, Solder joint fatigue models: review and applicability to chip scale packages, Microelectron. Reliab. 40 (200) 231–244.
[40] V. Vasudevan, X.J. Fan, An acceleration model for lead-free (SAC) solder joint reliability under thermal cycling, in: Proceedings of Electronic Components and Technology Conference (ECTC), 2008, pp. 139–145.